A Novel Method for the Vibration Optimisation of Structures Subjected to Dynamic Loading

David J. Munk[1,2], **Gareth A. Vio**[1] **and Grant P. Steven**[1]

[1]School of AMME, The University of Sydney
Building J11, Sydney, NSW, 2006, Australia

[2]e-mail: david.munk@sydney.edu.au

Keywords: Optimisation, Topology, Flutter, Evolutionary

Abstract. The optimum design of structures with frequency constraints is of great importance in the aeronautical industry. In order to avoid severe vibration, it is necessary to shift the fundamental frequency of the structure away from the frequency range of the dynamic loading. This paper develops a novel topology optimisation method for optimising the fundamental frequencies of structures. The finite element dynamic eigenvalue problem is solved to derive the sensitivity function used for the optimisation criteria. An alternative material interpolation scheme is developed and applied to the optimisation problem. A novel level-set criteria and updating routine for the weighting factors is presented to determine the optimal topology. The optimisation algorithm is applied to a simple two-dimensional plane stress plate to verify the method. Optimisation for maximising a chosen frequency and maximising the gap between two frequencies are presented. This has the application of stiffness maximisation and flutter suppression. The results of the optimisation algorithm are compared with the state of the art in frequency topology optimisation. Test cases have shown that the algorithm produces similar topologies to the state of the art, verifying that the novel technique is suitable for frequency optimisation.

1 INTRODUCTION

Optimal design against vibrations and noise has been undertaken some decades ago in the form of shape optimisation with respect to the fundamental and higher order eigenfrequencies of transversely vibrating beams [1, 2]. Subsequent papers focus on maximisation of the separation between two consecutive eigenfrequencies of the beam [3, 4]. A survey by Grandhi [5] covers the early developments in this area.

Vibration response is a design consideration of a structure subjected to dynamic loads [6]. For example, it is advantageous to keep the natural frequencies of the structure away from any driving frequencies that may be applied to the structure. Structures with a high fundamental frequency result in a stiff design which is good for static loads [7]. There have been cases where designers have underestimated the effects of the dynamic response, the most famous example being the Tacoma Narrows bridge in 1940, which collapsed due to resonance [8]; the problem being the frequency of the wind's gust differing little from the natural bending and twisting modes of the bridge deck [9]. This problem is not confined to bridge design. In aircraft structures the onset of flutter is a result of the coalescence of two natural frequencies resulting in zero damping ratio [10]. Therefore it is advantageous to design the supporting structure such that the natural frequencies are far enough apart to delay the onset of flutter.

There are several established structural topology optimisation algorithms in the literature. The first to be applied to frequency optimisation is the homogenization method, developed by Bendsoe and Kikuchi [11]. This method uses an anisotropic composite with micro-scale voids to represent the material. For a given case the optimal design is found by optimising these microstructures and their orientations. Diaz and Kikuchi [12] were the first to extend the homogenization method to vibrational optimisation. Subsequently, Ma *et al.* [13, 14, 15], Tenek and Hagiwara [16], Diaz *et al.* [17] and Krog [18] analysed the maximisation of multiple frequencies of freely vibrating disks and plates using the homogenization technique. Krog and Olhoff [7] apply a variable bound formulation to facilitate the treatment of multiple eigenfrequencies.

The first continuous structural topology optimisation technique was developed by Bendsoe [19] in 1989. The Solid Isotropic Material with Penalisation (SIMP) method represents the material properties by one design variable per element with a penalisation factor. The SIMP method was extended by Kosaka and Swan [20] to include optimisation of dynamic problems. However, it has been demonstrated that the SIMP model is unsuitable for frequency optimisation, as localised modes tend to appear in low density regions [21]. A modified SIMP model using a discontinuous function has been applied to vibrating continuum structures by Pedersen [21], Du and Olhoff [22] and Jensen and Pedersen [23]. Rubio *et al.* [24] applied SIMP topology optimisation for tailoring vibration mode shapes for the design of piezoelectric devices. These methods are derived from the Karush-Kuhn-Tucker (KKT) optimality conditions [25].

A popular non-gradient based optimisation algorithm is the Evolutionary Structural Optimisation (ESO) method, which uses a physical response function, such as the von Mises stress, to gradually remove regions of inefficient material [26]. Xie and Steven (1994) [27] were the first to extend the ESO method to include frequency optimisation. Xie and Steven [28] analysed dynamic problems using the ESO method. Zhao *et al.* [29] looked at frequency optimisation with lumped masses. Zhao *et al.* [30] performed optimisation for the natural frequencies of thin plate bending vibration problems. Yang *et al.* [31] applied the hard-kill BESO method to frequency optimisation problems. More recently Huang *et al.* [32] applied the soft-kill penalty based BESO method to frequency optimisation problems.

A recent structural topology optimisation algorithm, developed by Tong and Lin [33], called the Moving Iso-Surface Threshold (MIST) technique is a hybrid of: the ESO method, using a physics based function, the SIMP method, employs a moving level to define the element based design variables and the level set method, uses evolving material boundaries expressed as iso-values or levels. Vasista and Tong [34] demonstrated this method on pressurised cellular compliant mechanisms by adding a mixed u/P finite-element formulation alongside the MIST optimisiation. Vasista and Tong [35] apply the MIST topology optimisation method to aircraft structural design and extend the method to three-dimensional 'block' design. Munk *et al.* [36] extend the MIST algorithm to complex three-dimensional geometries, such as the internal configuration of a UAV wing, with structural cross-coupling.

This article presents a novel method for the topology optimisation of single and multiple eigenfrequencies of continuum structures. The optimisation method is an extension of the MIST algorithm [33] to the eigenvalue problem, with an alternative material interpolation scheme and level-set method. The objective of the work is to develop an improved optimisation algorithm for dynamic structures and compare with the current state of the art.

2 THEORETICAL ANALYSIS

This section outlines the optimisation algorithm of the paper. An overview of the MIST algorithm is given, followed by the structural model. The modifications to the method made for frequency optimisation is described followed by the convergence criteria.

2.1 Overview of Optimisation Algorithm

The optimisation problem being solved is one of the form:

$$\begin{aligned} \text{min: } & J(\mathbf{x}, t) \\ \text{s.t.: } & g_r(\mathbf{x}, t) = 0 \\ & g_s(\mathbf{x}, t) \leq 0 \\ & \mathbf{x}_l \leq \mathbf{x} \leq \mathbf{x}_u \end{aligned}$$

The aim is to find the optimum material layout, $\mathbf{x}$ values, to minimise the structural objective function, J, subjected to given finite element, g_r, and material, g_s, constraints. A physical response function Φ is calculated at all nodal points across the design domain. The physical response function is determined by the structural objective and gives the relative structural performance of all points in the domain. An iso-surface, S, intersects the physical response function forming the contour of the structural boundary (Figure 1).

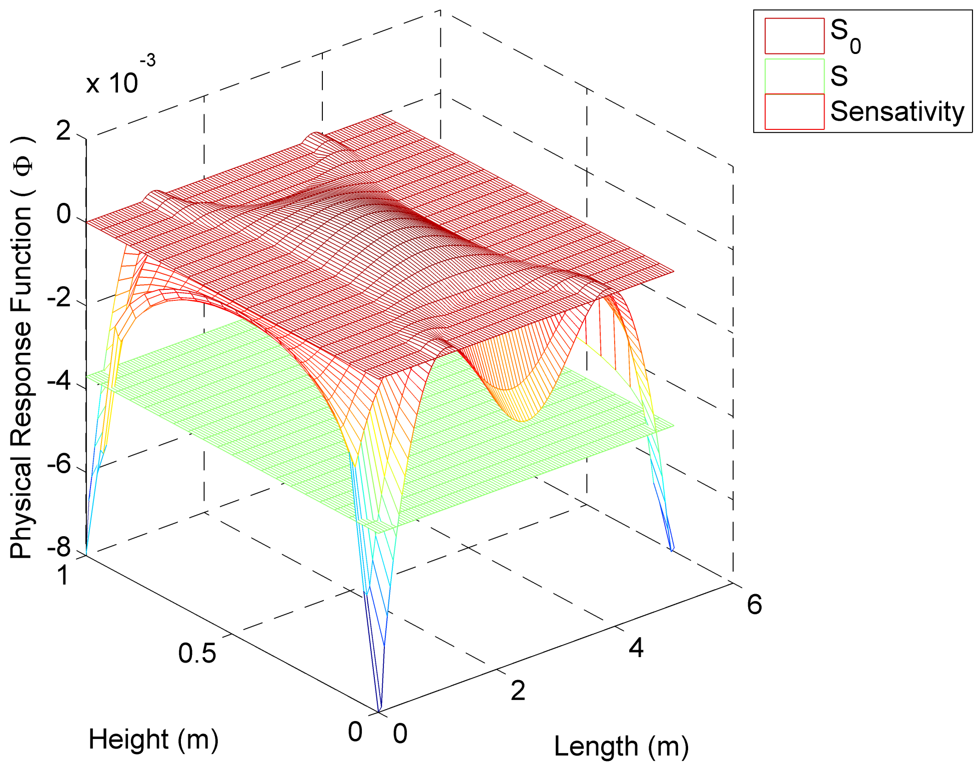

Figure 1: Physical Response Function for Clamped Beam

Weighting factors are applied to the elements to represent the material distribution. Void and solid elements are modeled by weighting factors of 0 and 1 respectively. In the optimisation update routine, the elements with all nodal physical response functions above the iso-surface move towards solid material, and the elements with all nodal physical response functions below the iso-surface move towards void material. For the elements with nodal physical response functions above and below the iso-surface, the weighting factor is a function of the projected area above the iso-surface (Section 2.5.).

2.2 Initialisation of Structural Model

The structural model must be defined before the optimisation can be started. The structural model is defined by a finite element mesh. The nodal co-ordinates, element connectivity table, node numbers connected to each element, and element areas based on the finite element mesh are stored. The global stiffness, K, and mass, M, matrices are extracted from the finite element solver. The element stiffness, K_e, and mass, M_e, matrices can then be calculated from these.

The problem of eigenvalue maximisation has a trivial solution: in principle an infinite eigenvalue can be obtained by removing the entire structure [6]. Therefore a volume constraint on the amount of material, f, is set. One weighting factor, x_i, is used per finite element, this is similar to the density design variable in the SIMP gradient based method [37]. For non-design areas, i.e. areas that are classified as either void or solid due to the design problem, the weighting factors for these elements are set to either 1 for solid or 0 for void. All the remaining weighting factors are initialised uniformly with an intermediate value that satisfies the material constraints. All the weighting factors are stored in vector **x**. The initial penalisation factor β is set. The material property model is initialised by defining values for: E_{solid}, E_{void}, ρ_{soild} and ρ_{void}. The stabilisation move limit, δ, and filter radius are also defined in the initialisation stage.

2.3 Frequency Optimisation Problem

In finite element analysis the dynamic response of a structure is represented by the following eigenvalue problem:

$$\left(\mathbf{K} - \omega_{nj}^2 \mathbf{M}\right) u_j = 0 \tag{1}$$

where $\mathbf{K}$ is the global stiffness matrix, $\mathbf{M}$ is the global mass matrix, ω_{nj} is the j^{th} natural frequency and u_j is the eigenvector corresponding to ω_{nj}. The natural frequency and the corresponding eigenvector are related to each other by the Rayleigh quotient:

$$\omega_{nj}^2 = \frac{k_{nj}}{m_{nj}} \tag{2}$$

where the modal stiffness k_{nj} and the modal mass m_{nj} are defined by:

$$k_{nj} = u_j^T \mathbf{K} u_j \tag{3}$$

$$m_{nj} = u_j^T \mathbf{M} u_j \tag{4}$$

For the topology optimisation problem of maximising the natural frequency ω_{nj} the problem can be stated as [38]:

$$\begin{aligned} &\text{maximise: } \omega_{nj} \\ \text{s.t.} \quad & V^* - \sum_{i=1}^{N_E} V_i x_i = 0 \\ & 0 \leq x_i \leq 1 \end{aligned} \tag{5}$$

where V_i is the volume of the i^{th} element and V^* is the predefined total structural volume. The objective function of the optimisation problem is ω_{nj}. From Equation (2), the sensitivity of the objective function can be calculated by:

$$\frac{d\omega_{nj}}{dx_i} = \frac{1}{2\omega_{nj}u_j^T\mathbf{M}u_j}\left[2\frac{\partial u_j^T}{\partial x_i}\left(\mathbf{K}-\omega_{nj}^2\mathbf{M}\right)u_j + u_j^T\left(\frac{\partial \mathbf{K}}{\partial x_i} - \omega_{nj}^2\frac{\partial \mathbf{M}}{\partial x_i}\right)u_j\right] \tag{6}$$

using the eigenvalue problem (Equation (1)) Equation (6) can be simplified to [39]:

$$\frac{d\omega_{nj}}{dx_i} = \frac{1}{2\omega_{nj}u_j^T\mathbf{M}u_j}\left[u_j^T\left(\frac{\partial \mathbf{K}}{\partial x_i} - \omega_{nj}^2\frac{\partial \mathbf{M}}{\partial x_i}\right)u_j\right] \tag{7}$$

The sensitivity number (Equation (7)) is an indicator for the change in the eigenvalue, ω_{nj}^2, as a result of the removal of the j^{th} element. It is effectively the gradient of the eigenvalue solution of the finite element problem. The gradient for each element must be calculated to develop the physical response function.

2.4 Alternative Material Interpolation Scheme

To obtain the gradient information of the design variable (Section 2.3.), the material properties must be interpolated between 0, void, and 1, solid material. The most simple material interpolation scheme is the power law penalisation scheme [40]:

$$E(x_i) = E_{solid}x_i^{\beta} \tag{8}$$

where β is the penalisation factor, defined in Section 2.2. However, this scheme results in numerical difficulties for the eigenvalue optimisation problem [21]. The main problem is that the extremely high ratio between mass and stiffness for small x_i and large β (greater than 1) causes artificial localised vibration modes in the low density regions. A method to avoid this issue is to keep the ratio between mass and stiffness constant at low x_i values by requiring that:

$$\rho(x_{min}) = \rho_{void}\rho_{solid} \tag{9}$$

$$E(x_{min}) = E_{void}E_{solid} \tag{10}$$

Therefore an alternative material interpolation scheme can be defined as:

$$\rho(x_i) = x_i\rho_{solid} + \rho_{void} \tag{11}$$

$$E(x_i) = \left[\frac{E_{void} - E_{void}^{\beta}}{1 - E_{void}^{\beta}}\left(1 - x_i^{\beta}\right) + x_i^{\beta}\right]E_{solid} \qquad (0 \leq x_i \leq 1) \tag{12}$$

By differentiating Equations (11) and (12) the derivatives of the global mass **M** and stiffness **K** matrices with respect to the weighting factors can be obtained:

$$\frac{\partial M}{\partial x_i} = M_{solid_i} \tag{13}$$

$$\frac{\partial K}{\partial x_i} = \frac{1 - E_{void}}{1 - E_{void}^{\beta}} \beta x_i^{\beta - 1} K_{solid_i} \tag{14}$$

where M_{solid_i} and K_{solid_i} are the i^{th} element mass and stiffness matrices when they are solid. Equations (13) and (14) can be substituted into Equation (7) to obtain the sensitivity number as a function of the material interpolation model.

$$\frac{d\omega_{nj}}{dx_i} = \frac{1}{2\omega_{nj}} u_j^T \left(\frac{1 - E_{void}}{1 - E_{void}^{\beta}} \beta x_i^{\beta - 1} K_{solid_i} - \omega_{nj}^2 M_{solid_i} \right) u_j \tag{15}$$

The sensitivity number for elements tending toward solid and void material can be explicitly expressed as:

$$\alpha_i = \frac{1}{\beta} \frac{d\omega_{nj}}{dx_i} \begin{cases} \frac{1}{2\omega_{nj}} u_j^T \left(\frac{1 - E_{void}}{1 - E_{void}^{\beta}} K_{solid_i} - \frac{\omega_{nj}^2}{\beta} M_{solid_i} \right) u_j & x_i = 1 \\ \frac{1}{2\omega_{nj}} u_j^T \left(\frac{E_{void}^{\beta - 1} - E_{void}^{\beta}}{1 - E_{void}^{\beta}} K_{solid_i} - \frac{\omega_{nj}^2}{\beta} M_{solid_i} \right) u_j & x_i \approx 0 \end{cases} \tag{16}$$

This material interpolation scheme is a ’soft-kill’ method, where the elements stiffness and densities are gradually reduced, i.e. elements are not completely removed or included.

2.5 Alternative Method for Calculating the Level of the Iso-Surface and Updating Weighting Factors

To calculate the element weighting factors the iso-surface level , t, must first be calculated using an iterative bi-section method. In this method the initial value of t is the average of the minimum and maximum value of the physical response function Φ. The difference between Φ and t is calculated at all nodes in the design domain. All the weighting factors in the design region are updated where i is the current element.

for $(\Phi - t) > 0$:

$$x_i = \begin{cases} 0 & \text{if } x_{i-1} < 0.1 \\ x_{i-1} - 0.1 & \text{otherwise} \end{cases} \tag{17}$$

for $(\Phi - t) < 0$:

$$x_w(i) = \begin{cases} 1 & \text{if } x_{i-1} > 0.9 \\ x_{i-1} + 0.1 & \text{otherwise} \end{cases} \tag{18}$$

The amount of material is summed $\sum_{i=1}^{N_E} (x_{ik} A_i)$ where A_i is the area of element i, k is the current iteration in the bi-section method and N_E is the total number of elements in the mesh. The summed material is then checked against the material constraint, $f A_{total}$ (where A_{total} is the total mesh area and f is a volume fraction) and the iso-value, t, is updated:

$$\text{if} \sum_{i=1}^{N_E} (x_{ik} A_i) > f A_{tot} \begin{cases} t_{min(k+1)} = t_k \\ t_{max(k+1)} = t_{max(k)} \end{cases}$$

or

$$\text{if} \sum_{i=1}^{N_E} (x_{ik} A_i) < f A_{tot} \begin{cases} t_{min(k+1)} = t_{min(k)} \\ t_{max(k+1)} = t_k \end{cases}$$

the iso-surface is then calculated by:

$$t_k = \begin{cases} \frac{t_{max(k)} + t_{min(k)}}{2} & S > 0 \\ 0 & S < 0 \end{cases} \tag{19}$$

after each iteration if the sensitivity numbers are all less than zero the iso-surface for the previous iteration is re-calculated by:

$$t_k = \frac{t_{max(k)} + t_{min(k)}}{2} \quad \text{where } t_{min(k)} = t_{k-1} \tag{20}$$

This process is repeated until the summed material is within a small tolerance ζ of the material constraint. For the non-design solid and/or void regions, the value of $\Phi - t_k$ is set to a positive number for solid regions and a negative number for void regions.

The updating procedure for elements with either all node values of $(\Phi - t_k) > 0$ or $(\Phi - t_k) < 0$ is given previously, however if $(\Phi - t_k) > 0$ at some node(s) and $(\Phi - t_k) < 0$ at other node(s), then x_{ik} is based on the ratio of projected positive area to total element area as seen in Figure 2. As can be seen from Figure 2 the positive area of the element is enclosed in the boundary

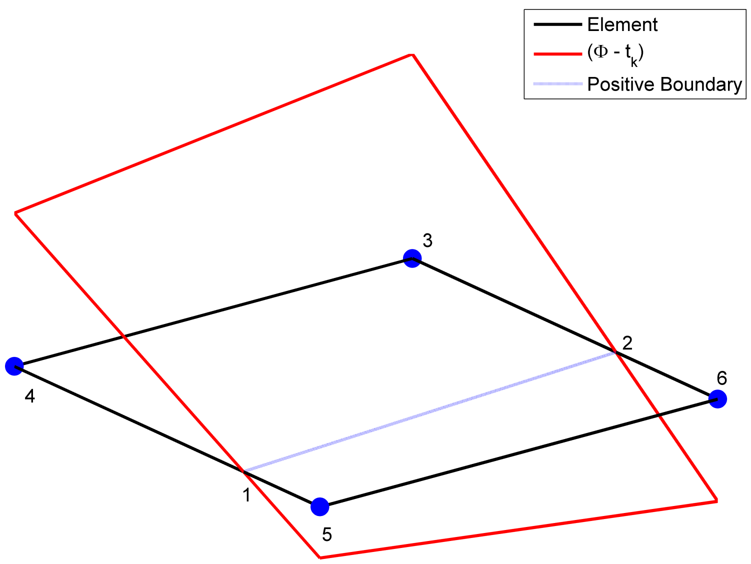

Figure 2: 3D View of Nodal Values of $(\Phi - t_k)$ for Element i

outlined by points 1-4. Therefore the weighting factor for the element shown in Figure 2 is given by:

$$x_{wk} = \frac{A_{ik}^{+}}{A_i} \tag{21}$$

To calculate the projected positive area, A_{ik}^{+}, the X_v and Y_v co-ordinates of the vertex, shown as points 1 and 2 in Figure 2, must be determined. This is done by determining the edge of the element that the vertex lies on, by seeing which edge has one node with a positive $(\Phi - t_k)$ and one node with a negative $(\Phi - t_k)$. Once the correct edge has been identified the co-ordinates of the vertex can be calculated by calculating the ratio of the positive and negative magnitudes:

$$\eta = \frac{|\Phi - t_k|_1}{|\Phi - t_k|_1 + |\Phi - t_k|_2} \tag{22}$$

the co-ordinates of the vertex can then be calculated by:

$$X_v = X_1 + \eta(X_2 - X_1) \tag{23}$$

$$Y_v = Y_1 + \eta(Y_2 - Y_1) \tag{24}$$

where the values with a subscript of 1 represent the nodes with a positive $(\Phi - t_k)$ value, and the values with a subscript of 2 represent the nodes with a negative $(\Phi - t_k)$ value. Once the co-ordinates of all the vertices of A_{ik}^{+} are determined, the area A_{ik}^{+} is determined using the standard method for determining the area of a non-self-intersecting arbitrary polygon using its vertex co-ordinate data [41]:

$$A_{ik}^{+} = \frac{1}{2} \sum_{v=i}^{N_v} (X_v Y_{v+1} - X_{v+1} Y_v) \tag{25}$$

where N_v is the number of vertices of A_{ik}^{+}, X_{N_v+1} and Y_{N_v+1} are equal to X_1 and Y_1 in order to close the polygon.

2.6 Convergence Criteria

Standard topology optimisation procedures determine the convergence of the solution when the change in each element weighting factor is less than a certain percentage, hence:

$$\Delta x = max\left(|x_{new} - x|\right) \tag{26}$$

This criterion can be too strict causing the optimiser to run without terminating even though the overall topology is unchanged. The convergence criteria can be relaxed by considering the change in the element weighting factor as a function of the area of the total design domain such that:

$$\Delta x = \frac{\sum_{i=1}^{N_E} \left(|x_{new_i} - x_i| A_i\right)}{\sum_{i=1}^{N_E} A_i} = \frac{\sum_{i=1}^{N_E} \left(|x_{new_i} - x_i| A_i\right)}{A_{total}} \tag{27}$$

This criteria (Equation (27)) is used to determine the convergence of the optimisation algorithm.

2.7 Filtering Schemes for Solid-Void Structures

The algorithm presented is a ’soft-kill’ method, hence a material interpolation scheme is required; i.e. elements are not completely removed. Therefore the final topologies produced are not solid-void structures. Multiple filtering schemes can be used to transform composite structures into solid-void topologies. The two methods used here are:

The mean filter:

$$x_{w_i} = \begin{cases} 0 & \text{if} \quad x_{w_i} < \bar{x}_w \\ 1 & \text{if} \quad x_{w_i} > \bar{x}_w \end{cases} \tag{28}$$

where $\bar{x}_w$ is the mean value of the weight function.

The median filter:

$$x_{w_i} = \begin{cases} 0 & \text{if} \quad x_{w_i} < \tilde{x}_w \\ 1 & \text{if} \quad x_{w_i} > \tilde{x}_w \end{cases} \tag{29}$$

where $\tilde{x}_w$ is the median value of the weight function. Initially a mean filter is used, as it does not favor higher or lower densities. However this may result in elements that are not connected to the main structure. In this case a median filter is used to remove all outliers.

3 RESULTS AND DISCUSSION

The results of the optimisation algorithm are presented in this section. To verify the algorithms optimality a two-dimensional plane stress rectangular plate is optimised for maximisation of the first natural frequency. This example has been optimised by both the ESO [28] and homogenization techniques [16], hence proving to be a good comparison for the new algorithm proposed in this article. Secondly, a plate wing is optimised for separation of the 2^{nd} and 3^{rd} natural frequencies to delay flutter. This is a simple example to verify the algorithms ability to increase the dynamic stability of a structure.

3.1 Rectangular Plate

Figure 3 shows the aluminium plate of dimensions $0.15m \times 0.1m$. The plate is fixed at two corners along its diagonal, with only in-plane vibration considered. A Young's modulus $E = 70GPa$, Poisson's ratio $\nu = 0.3$, thickness $t = 0.01m$ and density $\rho = 2700\frac{kg}{m^3}$ are defined for the plate. The domain is divided into 45 x 30 square plate elements. Using the method outlined

Figure 3: Rectangular Plate Under Plane Stress Conditions

in Section 2 the first natural frequency is increased until the volume constraint is met. As a result the history of the first natural frequency is obtained as shown in Figure 4. After 11 iterations,

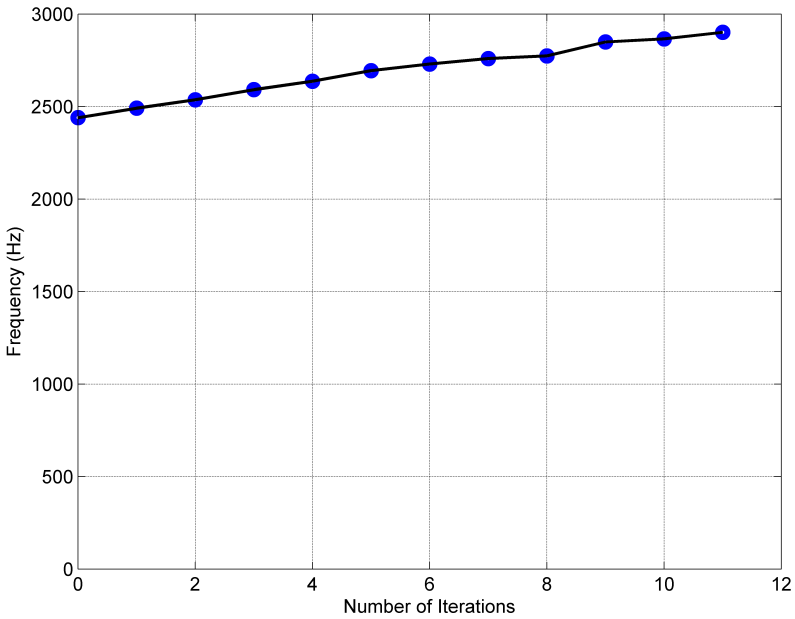

Figure 4: History of the First Natural Frequency of the Rectangular Plate

60% of the material is removed and the first frequency has been increased by approximately 20% from $2439.7Hz$ to $2901.1Hz$. The corresponding new design is given in Figure 5.

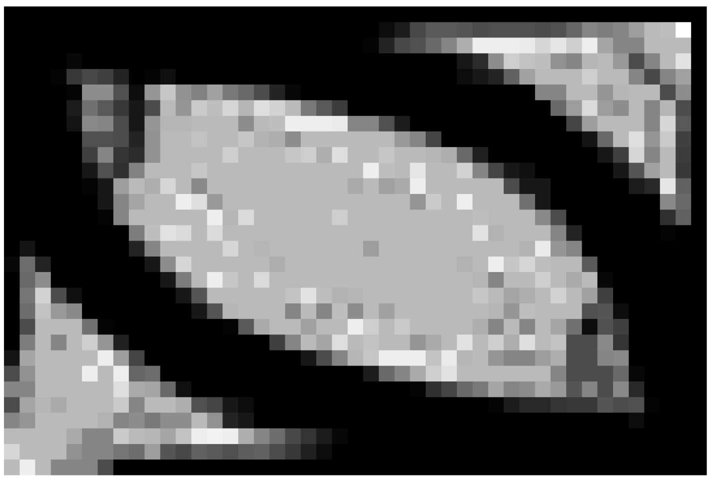

Figure 5: A New Composite Design for the Rectangular Plate with Increased First Frequency

Figure 5 shows the result of the optimisation algorithm for a composite design, i.e. with intermediate material. For manufacturing purposes a solid-void or 1-0 structure is required. Therefore the design shown in Figure 5 can be filtered to produce a 1-0 structure as shown in Figure 6.

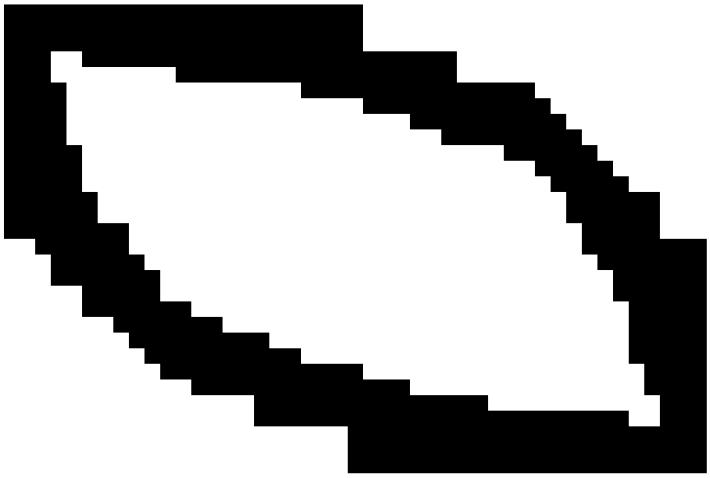

Figure 6: A New Solid-Void Design for the Rectangular Plate with Increased First Frequency

Figure 6 shows a design which has the same topology as the designs obtained by the homegenization method [16] and the ESO method [39]. Since the ESO method only removes 8 elements at every iteration this method is significantly slower, taking 85 iterations to remove 50% of the structure compared with 11 for this method. This result gives confidence to the method for optimisation of maximum frequency. However, there is no control as to what is happening to the other frequencies during the optimization process. This can lead to other frequencies dropping below their initial values. Such behaviour is undesirable in structural mechanics (see Section I). This can be avoided, or at least delayed, by instead of maximising the first natural frequency, maximise the gap between neighboring frequencies. This method will be demonstrated in the next section on a wing structure.

3.2 Plate Wing

Figure 7 shows the aluminium plate wing of dimensions $0.25m \times 1m$. The plate is fixed along one of its edges, to represent a cantilever wing. A Young's modulus $E = 70GPa$, Poisson's ratio $\nu = 0.3$, thickness $t = 0.001m$ and density $\rho = 2700\frac{kg}{m^3}$ are defined for the plate. The domain is divided into 26 x 101 square plate elements. Since the span and chord dimensions

Figure 7: Cantilever Plate Wing

must remain consistent the volume constraint for this optimisation problem is set to 85%. The novel optimisation method of this paper is used to increase the gap between the 2^{nd} and 3^{rd} natural frequencies, as they are the closest before optimisation. As a result the optimisation history of the difference between the 2^{nd} and 3^{rd} natural frequencies is shown in Figure 8. After 8

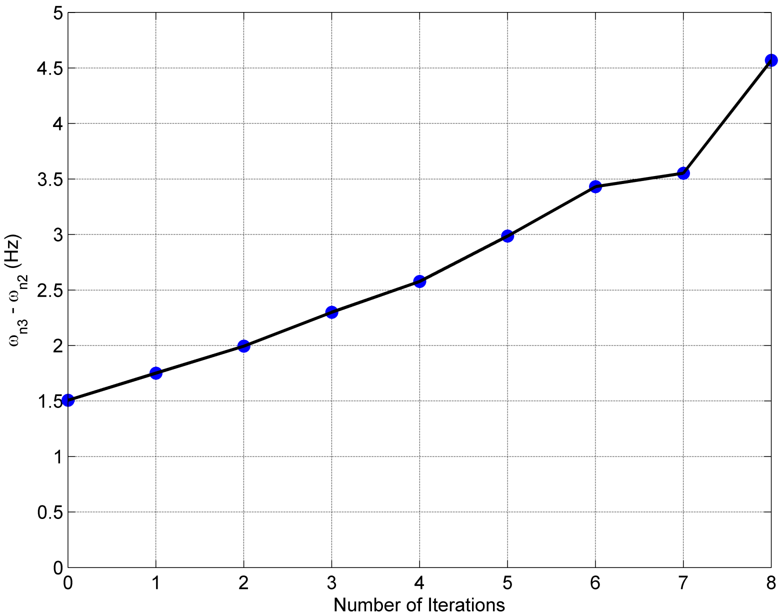

Figure 8: History of the Difference Between the 2^{nd} and 3^{rd} Natural Frequencies for the Cantilever Wing

iterations, 15% of the material is removed and the gap between the 2^{nd} and 3^{rd} natural frequencies has been increased by over 200% from $1.5Hz$ to $4.6Hz$. The corresponding new design, before filtering is performed, can be seen in Figure 9. Figure 9 gives the optimal topology for a composite wing design. For manufacturing purposes and the experimental analysis (Section 3.3.) a solid-void structure is required. Therefore the design given in Figure 9 can be filtered to produce a solid-void structure as shown in Figure 10. Figure 10 shows a symmetrical structure that has removed material from the leading and trailing edges toward the tip. The second natural frequency corresponds to the second bending mode and the third natural frequency corresponds to the first twisting (torsional) mode. Therefore the removal of material from either edge is done to increase the frequency of the twisting mode, while having minimal effect on the second bending mode. The structure starts to build up again as the tip of the wing is approached (Figure 10), this keeps the frequency of the second bending mode relatively constant such that it does not approach the first mode.

The 2^{nd} and 3^{rd} mode for the wing before and after the optimisation is performed can be seen in Figures 11 and 12. The majority of the removed material in the optimisation process occurs after the maximum bending displacement (Figure 11). This results in minimal change of the 2^{nd} natural frequency, to avoid coupling the 1^{st} and 2^{nd} mode. The resulting 'I' beam shape towards the tip, reduces the inertia in the 'twisting' dimension, thus increasing the 3^{rd} natural frequency (Figure 12). This results in an increased frequency difference between all modes.

The goal of this problem was to delay the onset of flutter for the plate wing (Figure 7). The flutter velocity of the wing before optimisation is $13.88ms^{-1}$. The flutter velocity after the wing has been optimised is increased by approximately 20% to $16.56ms^{-1}$. Therefore it is

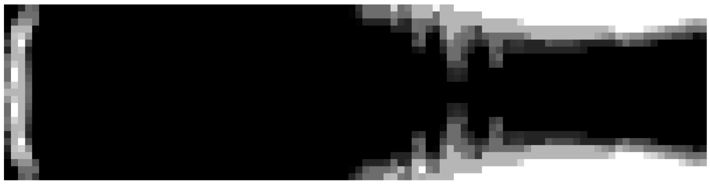

Figure 9: A New Composite Design for a Wing with Increased Difference in 2^{nd} and 3^{rd} Natural Frequencies

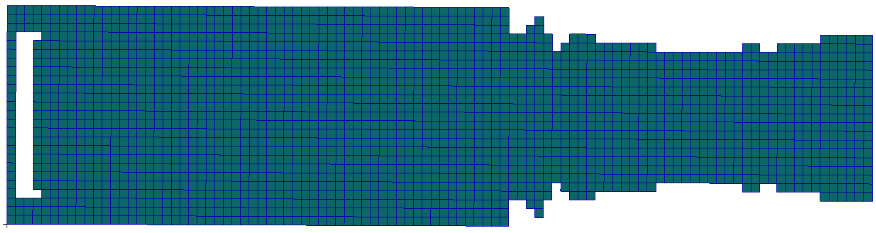

Figure 10: A New Solid-Void Design for a Wing with Increased Difference in 2^{nd} and 3^{rd} Natural Frequencies

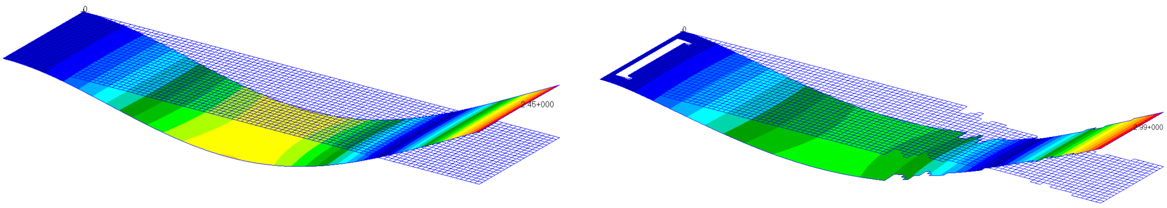

Figure 11: 2^{nd} Mode Shape of Final and Initial Wing Structure

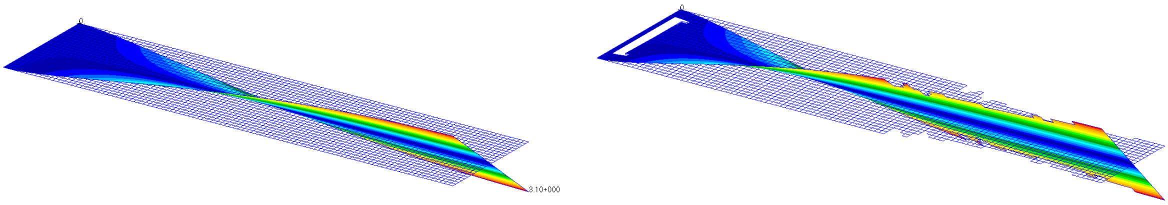

Figure 12: 3^{rd} Mode Shape of Final and Initial Wing Structure

clear that the novel optimisation method presented in this article is effective for delaying flutter and can be successfully used for maximising the difference between frequencies.

4 CONCLUSIONS

A novel method for the optimisation of the fundamental frequencies of structures has been presented. The maximisation of the 1^{st} natural frequency and increasing the gap between two coinciding frequencies for increasing dynamic stability has been demonstrated. A novel level-set criteria and updating routine for the weighting factors was developed to determine the optimal topologies.

The optimised rectangular plate has an increased 1^{st} natural frequency of approximately 20%, $2901.1Hz$ compared to $2439.7Hz$ for the initial design, with a weight saving of 60%. The resulting topology is comparable to those determined using the homogenization and ESO techniques. Proving to be a good test case that verifies the novel method.

The optimised plate wing has an increase of over 200%, $4.6Hz$ compared to $1.5Hz$, in the difference between the 2^{nd} and 3^{rd} natural frequencies. This resulted in a 20% increase in the flutter velocity of the wing, $16.56ms^{-1}$ compared to $13.88ms^{-1}$. Therefore confirming the novel optimisation techniques ability to delay the onset of flutter and create structures that are more dynamically stable. These results add to the work done in dynamic optimisation problems [12, 20, 27].

5 COPYRIGHT STATEMENT

6 REFERENCES

[1] N. Olhoff. Optimization of vibrating beams with respect to higher order natural frequencies. *J. Struc. Mech.*, 4:87–122, 1976.

[2] N. Olhoff. Maximizing higher order eigenfrequencies of beams with constraints on the design geometry. *J. Struc. Mech.*, 5:107–134, 1977.

[3] N. Olhoff and R. Parbery. Designing vibrating beams and rotating shafts for maximum difference betwen adjacent natural frequencies. *Int. J. Solids Struct.*, 20:63–75, 1984.

[4] M. P. Bendsoe and N. Olhoff. A method of design against vibration resonance of beams and shafts. *Optim. Control Appl. Methods*, 6:191–200, 1985.

[5] R. V. Grandhi. Structural optimization with frequency constraints - a review. *AIAA Journal*, 31:2296–2303, 1993.

[6] M. P. Bendsoe and O. Sigmund. *Topology Optimization Theory, Methods and Applications*. Springer, first edition, 2003.

[7] L. A. Krog and N. Olhoff. Optimum topology and reinforcement design of disk and plate structures with multiple stiffness and eigenfrequency objectives. *Computers and Structures*, 72:535–563, 1999.

[8] T. von Karman. Collapse of the tacoma narrows bridge. *Resonance*, 10:97–102, 2005.

[9] R. D. Blevins. *Flow-Induced Vibration*. Krieger Publishing Company, second edition, 2001.

[10] R. L. Bisplinghoff and H. Ashley. *Principles of Aeroelasticity*. Wiley, New York, first edition, 1962.

[11] M. P. Bendsoe and N. Kikuchi. Generating optimal topology in structural design using a homogenization method. *Computer Methods in Applied Mechanics and Engineering*, 71:197–224, 1988.

[12] A. R. Diaz and N. Kikuchi. Solutions to shape and topology eignvalue optimization problems using a homogenization method. *Int. J. Numer. Meth. Engng*, 35:1487–1502, 1992.

[13] Z. D. Ma, N. Kikuchi, H. C. Cheng, and I. Hagiwara. Topology and shape optimization methods for structural dynamic problems. *In: P. Pedersen Optimal Design with Advanced Materials*, Elsevier Science Publishers:247–261, 1993.

[14] Z. D. Ma, H. C. Cheng, and N. Kikuchi. Structural design for obtaining desired eigenfrequencies by using the topology and shape optimization method. *Comput. Sys. Eng.*, 5:77–89, 1994.

[15] Z. D. Ma, N. Kikuchi, and H. C. Cheng. Topological design for vibrating structures. *Comput. Methods Appl. Mech. Eng.*, 121:259–280, 1995.

[16] L. H. Tenek and I. Hagiwara. Static and vibrational shape and topology optimization using homogenization and mathematical programming. *Comput. Methods Appl. Mech. Eng.*, 109:143–154, 1993.

[17] A. R. Diaz, R. Lipton, and C. A. Soto. A new formulation of the problem of optimum reinforcement of reissner-midlin plates. *Comp. Meth Appl. Mechs Eng.*, 123:121–139, 1994.

[18] L. A. Krog. Layout optimization of disk, plate, and shell structures. Technical report, University of Denmark, 1996.

[19] M. P. Bendsoe. Optimal shape design as a material distribution problem. *Structural Optimization*, 1:193–202, 1989.

[20] I. Kosaka and C. C. Swan. A symmetry reduction method for continuum structural topology optimization. *Comput. Struct.*, 70:47–61, 1999.

[21] N. L. Pedersen. Maximization of eigenvalues using topology optimization. *Struc. Multidisc. Optim.*, 20:2–11, 2000.

[22] J. Du and N. Olhoff. Topological design of freely vibrating continuum structures for maximum values of simple and multiple eigenfrequencies and frequency gaps. *Struc. Multidisc. Optim.*, 34:91–110, 2007.

[23] J. S. Jensen and N. L. Pedersen. On maximal eigenfrequency seperation in two-material structures. *J. Sound Vib.*, 289:967–986, 2006.

[24] W. M. Rubio, G. H. Paulino, and E. C. M. Silva. Tailoring vibration mode shapes using topology optimization and functionally graded material concepts. *Smart Materials and Structures*, 20, 2011.

[25] N. M. Patel, D. Tillotson, J. E. Renaud, A. Tover, and K. Izui. Comparative study of topology optimization techniques. *AIAA Journal*, 46:1963–1975, 2008.

[26] Y. M. Xie and G. Stevens. A simple evolutionary procedure for structural optimisation. *Computers and Structures*, 49:885–896, 1993.

[27] Y. M. Xie and G. P. Steven. A simple approach to structural frequency optimization. *Computers and Structures*, 53:1487–1491, 1994.

[28] Y. M. Xie and G. P. Steven. Evolutionary structural optimization for dynamic problems. *Computers and Structures*, 58:1067–1073, 1996.

[29] C. Zhao, G. P. Steven, and Y. M. Xie. Evolutionary natural frequency optimization of two dimensional structures with nonstructural lumped masses. Technical report, Finite Element Analysis Research Centre, The University of Sydney, 1995.

[30] C. Zhao, G. P. Steven, and Y. M. Xie. Evolutionary natural frequency optimization of thin plate bending vibration problems. *Struct. Optim.*, 11:244–251, 1996.

[31] X. Y. Yang, Y. M. Xie, G. P. Steven, and O. M. Querin. Topology optimization for frequencies using an evolutionary method. *J. Struc. Engng.*, 125:1432–1438, 1999.

[32] X. Huang, Z. H. Zuo, and Y. M. Xie. Evolutionary topological optimization of vibrating continuum structures for natural frequencies. *Eng. Comput.*, 88:357–364, 2010.

[33] L. Tong and J. Lin. Structural topology optimisation with implicit design varible-optimality and algorithm. *Finite Elements in Analysis and Design 47*, pages 922–932, 2011.

[34] S. Vasista and L. Tong. Topology-optimized design and testing of a pressure-driven morphing-aerofoil trailing-edge structure. *AIAA Journal*, 51:1898–1907, 2013.

[35] S. Vasista and L. Tong. Topology optimisation via the moving iso-surface threshold method: Implementation and application. *The Aeronautical Journal*, 118:315–342, 2014.

[36] D. J. Munk, G. A. Vio, and G. Steven. Structural optimisation of a conventional uav wing, using the moving iso-surface threshold technique. *submitted to Advances in Aerospace Science and Technology*, 2015.

[37] M. P. Bendsoe and O. Sigmund. Material interpolation schemes in topology optimisation. *Archieve of Applied Mechanics*, 69:635–654, 1999.

[38] X. Huang and Y. M. Xie. *Evolutionary Topology Optimization of Continuum Structures*. John Wiley and Sons, 2010.

[39] Y. M. Xie and G. P. Stevens. *Evolutionary Structural Optimization*. Springer, 1997.

[40] O. Sigmund and J. Petersson. Numerical instabilities in topology optimization: a survey on procedures dealing with checkerboards, mesh-dependecies and local minima. *Struct. Optim.*, 16:68–75, 1998.

[41] D. Zwillinger. *CRC Standard Mathematical Tables and Formulae*. Chapman and Hall / CRC Press: Boca Raton, FL, United States, 2003.